Eur Biophys J (2001) 30: 313–318
DOI 10.1007/s002490100165

ARTICLE

**Valeria Mollica · Alberto Borassi · Annalisa Relini
Ornella Cavalleri · Martino Bolognesi · Ranieri Rolandi
Alessandra Gliozzi**

# An atomic force microscopy investigation of protein crystal surface topography

Received: 20 December 2000 / Revised version: 2 May 2001 / Accepted: 2 May 2001 / Published online: 21 June 2001


**Abstract** Tapping mode atomic force microscopy was employed to study the surface structure of different protein crystals in a liquid environment. The (101) face of hen egg-white lysozyme crystals and the (111) face of horse spleen ferritin crystals were studied. On the (101) face of lysozyme crystals we observed islands delimitated by micro-steps and elongated in the [010] direction. The elongation direction coincides with the preferential growth direction predicted by a growth model reported in the literature. The islands observed on the ferritin (111) face are also delimitated by micro-steps but have circular symmetry. Sectioning of the images allowed us to measure the step heights. The surface free energy was estimated from the growth step morphology. Molecular resolution was achieved for ferritin crystals, showing a hexagonal surface packing, as expected for the molecular lattice of a (111) face in a fcc crystal.

**Keywords** Atomic force microscopy · Protein crystals · Crystal growth · Ferritin · Lysozyme

## Introduction

Since the pioneering work of Durbin and Carlson (Durbin and Carlson 1992; Durbin et al. 1993), several studies have shown that the atomic force microscope (AFM) is a useful tool to characterize protein crystals. Its ability to operate in a liquid environment is crucial to maintain protein crystal integrity and allows growth to be followed in situ (Durbin et al. 1993; Land et al. 1995; Malkin et al. 1995; Yip and Ward 1996; Land et al. 1997; Malkin et al. 1997; Yip et al. 1998a, 1998b).

In this work we used atomic force microscopy to investigate the surface morphology of hen egg-white lysozyme and horse spleen ferritin crystals. Lysozyme is a 15 kDa enzyme endowed with antibacterial action, due to its ability to hydrolyze various polysaccharides, especially those of bacterial cell walls. Hen egg-white lysozyme consists of a single polypeptide chain of 129 amino acids, which has been crystallized in a tetragonal lattice. While the (110) face of lysozyme crystals has been thoroughly characterized by AFM inspection (Durbin et al. 1993; Konnert et al. 1994; Li et al. 1999), the (101) face, here considered, has become an object of quantitative study by AFM only recently (Malkin et al. 1999). Other techniques, such as electron microscopy and video microscopy have previously been used to obtain information on growth steps (Durbin and Feher 1990) and growth rates (Forsythe et al. 1994, 1999).

Ferritin is a 470 kDa protein responsible for iron storage. It does not provide specific binding sites for Fe atoms; instead, it collects them in an internal inorganic matrix. It is formed by 24 identical subunits, each of 174 residues, assembled into a nearly spherical shell (~12 nm in diameter), thus providing a cavity where up to 4500 Fe atoms can be stored as insoluble Fe(III) hydroxide. Ferritin crystallizes in a cubic lattice, which reflects the high symmetry of the repeating protein oligomer. Crystals display an octahedral habit; therefore, all faces are equivalent, corresponding to (111) crystal planes. Being well known and characterized by X-ray diffraction, ferritin is currently used as a calibration standard for electron microscopy, being also employed as a model system to study specific antibody-antigen interactions for biosensor applications (Allen et al. 1997, 1998; Perrin et al. 1997). In addition, ordered two-dimensional arrays of ferritin could be formed on a solid support and imaged with the AFM at the molecular level (Ohnishi et al. 1992; Furuno et al. 1998), achieving resolution of the protein quaternary structure (Ohnishi et al. 1993). Because of the oligomer large size and high packing symmetry, ferritin

V. Mollica · A. Borassi · A. Relini (✉) · O. Cavalleri
M. Bolognesi · R. Rolandi · A. Gliozzi
Istituto Nazionale per la Fisica della Materia and
Dipartimento di Fisica, Università di Genova,
Via Dodecaneso 33, 16146 Genoa, Italy
E-mail: relini@fisica.unige.it

A. Borassi · M. Bolognesi
Advanced Biotechnology Center,
Largo R. Benzi 10, 16132 Genoa, Italy

crystal faces represent an interesting system for AFM inspection. In the present communication we show the results obtained by imaging the crystal (111) face at low resolution and at the molecular level, and compare them with those obtained for lysozyme.

## Materials and methods

Hen egg-white lysozyme and horse spleen ferritin were purchased from Sigma Aldrich (Milan, Italy). Lysozyme was dissolved in water at a concentration of 40 mg $mL^{-1}$; ferritin was purchased as a 100 mg $mL^{-1}$ aqueous solution and was further diluted to 25 mg $mL^{-1}$. In both cases the protein solution was centrifuged at 12,000×*g* for 15 min ($T = 4$ °C) and the supernatant was collected.

Crystals were grown by vapor diffusion techniques (sitting drop geometry) on prepared Plexiglass disks, at room temperature. The best adhesion between Plexiglass and the crystal surfaces was obtained on disks cut from a rod, without any further polishing. The crystallization droplet was composed of 4 μL protein solution and 4 μL reservoir solution. The reservoir solution contained 0.9 M NaCl in 0.1 M sodium acetate buffer, pH 4.6, for lysozyme, and 1.0 M ammonium sulfate, 0.08 M cadmium sulfate, 0.003 M sodium azide, in 0.02 M sodium acetate buffer, pH 5.8, for ferritin, respectively. Crystals suitable for AFM inspection (about 0.2 mm in each direction) were usually obtained after 12–36 h. Lysozyme was crystallized in a tetragonal lattice with unit cell dimensions $a = b = 7.91$ nm, $c = 3.79$ nm, space group $P4_32_12$ (PDB entry 1HEL). Ferritin crystallizes in a cubic lattice, with unit cell dimensions $a = b = c = 18.4$ nm, space group $F432$ (PDB entry 1IER).

Samples were rinsed with the reservoir solution in order to remove the crystals not adhering to the substrate and were immediately transferred to the AFM fluid cell. The AFM, a Nanoscope III with a Dimension 3000 stage (Digital Instruments), equipped with a "G" scanning head (maximum scan area 70×70 $\mu m^2$), was in a vibration-insulated environment. In the Dimension 3000 stage the cantilever is mounted on the piezo *xyz* translator. The standard fluid cell of the Dimension 3000 is not sealed and a ring of the solution surface remains exposed. A limited evaporation of the solvent occurred during the measurements, but we did not observe any effect on the crystal face structure on the time scale of the measurements (usually, 1–3 h). A video microscope integrated into the AFM allowed proper positioning of the AFM stylus and selection of crystal faces which were close to horizontal. Crystal faces were imaged in tapping mode using V-shaped $Si_3N_4$ cantilevers (200 μm length, nominal spring constant 0.06 N $m^{-1}$, nominal tip radius of curvature 20–40 nm, type DNP-S, Digital Instruments). Optimal imaging conditions were achieved at drive frequencies around 6 kHz and a scan rate of 0.7 Hz. Horizontal displacements were calibrated using a 10 μm pitch diffraction grating. The *Z* scale was calibrated by measuring the depth of the grating notches (180 nm) and the half unit cell steps (1 nm) obtained by scratching freshly cleaved mica with sandpaper (no. 1200). Assuming a linear behavior of the calibration factor, a suitable correction factor for heights on the order of 10 nm was then obtained. Roughness measurements were performed on different image sections with Digital Instruments Nanoscope Software version 4.23r4. Before measuring the roughness, image planefitting was performed to correct for the tilt of the crystal faces.

To measure the step heights, images could not be corrected for the face tilt by using software options such as "Planefit" or "Flatten", since these options fit the scan lines with polynomials, subtracting them from the image, and may slightly alter the height data. Such an effect is not important for roughness values, which are anyhow used in this work only for the purpose of comparison, but can be crucial if a precise measurement of the step height is sought. Raw images were therefore exported as ASCII files and sectioned along the scan lines to obtain surface profiles. The matrix entries were converted to height values in nanometers by means of a correction factor, taking into account the piezo characteristics and *z* range. The profile slope was evaluated from smooth regions of the profile. Each profile was then rotated for tilt correction and the step heights were evaluated.

## Results and discussion

A tapping mode image of the (101) face of a lysozyme crystal shows the presence of elongated islands (Fig. 1). The (101) face was selected by using the video microscope integrated into the AFM, on the basis of the external morphology of the crystal. The video microscope also allowed us to know the fast scan direction orientation with respect to the face edges. The terrace elongation direction is the [010] direction. The terrace morphology seems to suggest that growth occurs by two-dimensional nucleation. However, since individual molecules could not be resolved, it is also possible that structural imperfections in the lattice, such as edge dislocations, could give rise to new islands on the surface.

Surface anisotropy is quantitatively described by line roughness differences. We calculated the roughness of the surface profiles obtained by sectioning the image along different directions. The log-log plot of the line

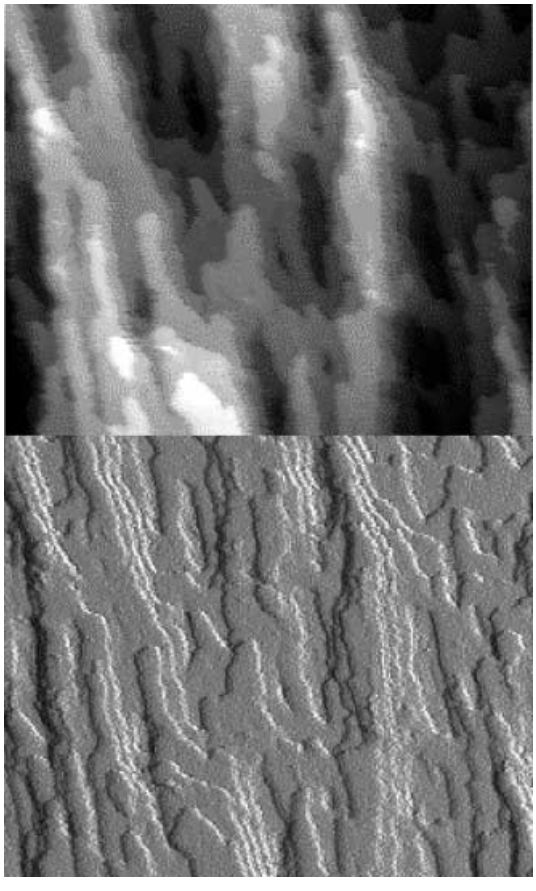

**Fig. 1** Low-resolution tapping mode AFM image in liquid environment of a lysozyme (101) crystal face, revealing growth islands. *Top*: height data, *z* range 200 nm; *bottom*: amplitude data, *z* range 7 nm. Image area 2.5×2.1 $\mu m^2$. Islands are elongated in the [010] direction

roughness versus the section length $r$ is shown in Fig. 2. The roughness values obtained along the terrace elongation direction turned out to be smaller than the values obtained perpendicular to the former direction (Fig. 2), confirming the visual impression that the terraces are larger along the elongation direction. Figure 2 also shows that for both directions the roughness follows a scaling law r.m.s.$\sim r^{\alpha}$ but with different exponents, namely $\alpha_1 = 0.20 \pm 0.04$ along the terrace elongation direction and $\alpha_2 = 0.52 \pm 0.05$ perpendicularly to it, as obtained by linear fit of the data in Fig. 2. No saturation of the roughness with the section length was observed, indicating that in this case the in-plane correlation length is larger than the scan size used in the AFM measurements.

Our observation of islands elongated in the [010] direction is in agreement with previous results. Islands elongated in the faster growth direction were reported by Durbin and Carlson (1992), both for (110) and (101) faces. Nadarajah and Pusey (1996) proposed a model for lysozyme crystal growth which associates the preferential growth direction on the (110) face with the presence of two periodic bond chains with respect to only one in the perpendicular direction. This model predicts only one periodic bond chain on the (101) face, and it is along the [010] direction.

A prolonged AFM scan on the crystal face favored growth in the fast scan direction. In fact, after 6 h from the engagement the terraces appeared smeared out and elongated in the fast scan direction (Fig. 3). It is likely that the AFM tip drags and afterwards releases some material along this direction.

The step height was measured considering many sections, in different images, and correcting for the crystal face tilt, as described in Materials and methods. The histogram of the step heights, showing a bimodal distribution, is shown in Fig. 4. A bimodal Gaussian fit yields step values of $3.1 \pm 0.1$ nm and $6.7 \pm 0.2$ nm. These values are in good agreement with the expected

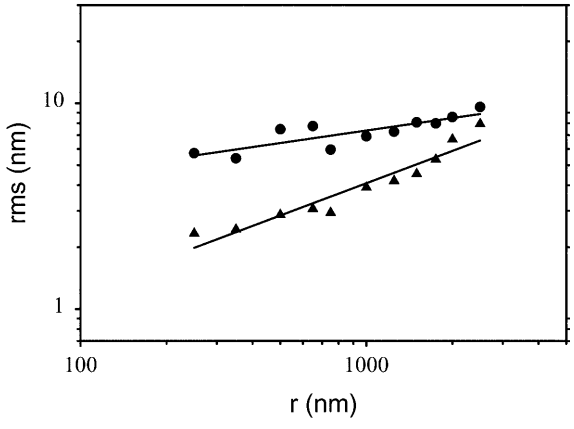


**Fig. 2** Log-log plot of line roughness versus section length for the lysozyme (101) crystal face. Roughness values were obtained from image sections along the terrace elongation direction (*triangles*) and perpendicular to this direction (*circles*). Each point is the mean value of nine different measurements. The *solid lines* are linear regressions of each set of experimental data. The resulting slopes, $\alpha_1 = 0.20 \pm 0.04$ in the terrace elongation direction and $\alpha_2 = 0.52 \pm 0.05$ perpendicularly, represent the corresponding roughness scaling exponents

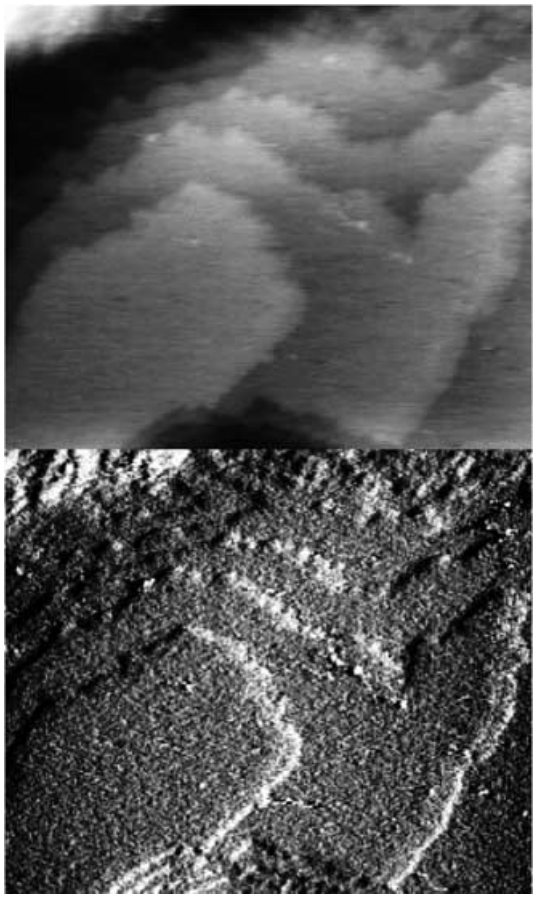

**Fig. 3** Tapping mode AFM image of a lysozyme (101) crystal face after 6 h from the engagement. *Top*: height data, $z$ range 84 nm; *bottom*: amplitude data, $z$ range 1.3 nm. Image area 2.5×2.1 μm$^2$. Terraces appear smeared out in the fast scan direction, which forms an angle of about 45° with the [010] direction

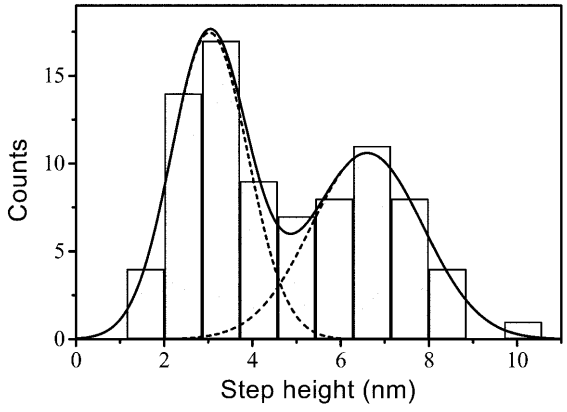


**Fig. 4** Histogram of the step height measured on different sections of raw height images of the lysozyme (101) crystal face. The total number of observations is 83. Sections were processed as described in Materials and methods in order to correct for the tilt of the crystal face. *Solid line*: bimodal Gaussian fit of the histogram, providing step heights of $3.1 \pm 0.1$ nm and $6.7 \pm 0.2$ nm

values for monomolecular and bimolecular steps in the (101) crystal face (3.4 and 6.8 nm), calculated from the tetragonal lysozyme crystal unit cell parameters. The step height frequencies in Fig. 4 indicate that, contrary to the (110) face, the growth layers in the (101) face are predominately one molecule thick, as observed previously by electron microscopy (Durbin and Feher 1990) and by AFM (Malkin et al. 1999). Actually, the theoretical analysis of lysozyme crystal growth (Nadarajah and Pusey 1996) indicated that for this face the crystallizing unit should be a helical tetramer with each molecule translated 1/4 unit along the helix axis from the previous one. Attachment of tetramers is then expected to give rise to monolayer growth.

Figure 5 is a 2.5×2.1 $\mu m^2$ image of a ferritin crystal surface. Roundish growth islands are visible. Clusters of molecules are dispersed on the islands, suggesting a nucleation growth process caused by the large supersaturation value of the growth solution (vide infra). The circular symmetry of the surface structures suggests the absence of a preferential growth direction. This is confirmed by a quantitative analysis of the line roughness, which turns out to be independent of the direction. The log-log plot of the line roughness versus the section length $r$ is given in Fig. 6. The roughness increases with $r$ up to a cutoff length scale of approximately 1 μm, after which it remains constant at approximately 17 nm. This cutoff length scale represents the in-plane correlation length (Barabási and Stanley 1995; Basu et al. 1999), which would correspond to the size of a cluster of islands (Fig. 5). The roughness saturation value should correspond to the molecular length (Barabási and Stanley 1995; Basu et al. 1999); in fact, the value obtained is comparable, within the experimental error, with the size of a ferritin oligomer. A linear fit of the data in the non-saturated region yields a scaling exponent $\alpha = 0.56 \pm 0.05$.

The histogram of step heights and its Gaussian fit are given in Fig. 7. This fit yields a step height of $10.5 \pm 0.6$ nm, which nicely agrees with the distance between adjacent (111) planes in the fcc lattice (10.5 nm) calculated from the ferritin crystal unit cell spacing measured by X-ray diffraction. Therefore, the steps observed correspond to single molecular layers.

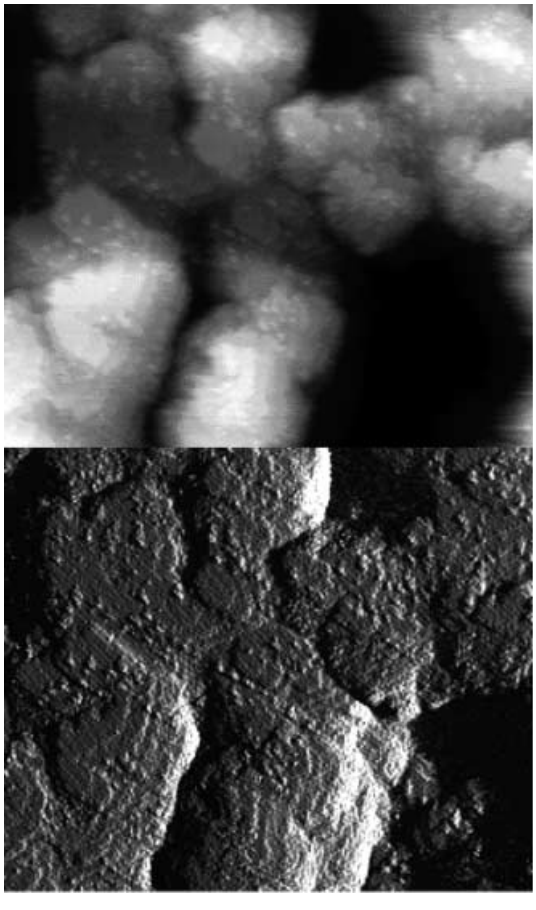

**Fig. 5** Low-resolution tapping mode AFM image in liquid environment of a ferritin (111) crystal face, revealing growth islands. *Top*: height data, $z$ range 320 nm; *bottom*: amplitude data, $z$ range 3.0 nm. Image area 2.5×2.1 $\mu m^2$

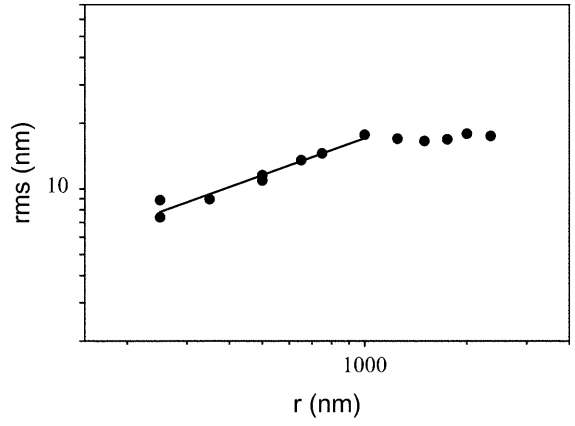


**Fig. 6** Log-log plot of roughness versus section length for a ferritin (111) crystal face. Each point is the mean value of 15 different measurements. A linear regression (*solid line*) of the experimental data was performed in the region before the saturation is reached. The resulting slope, $\alpha = 0.56 \pm 0.05$, represents the corresponding roughness scaling exponent

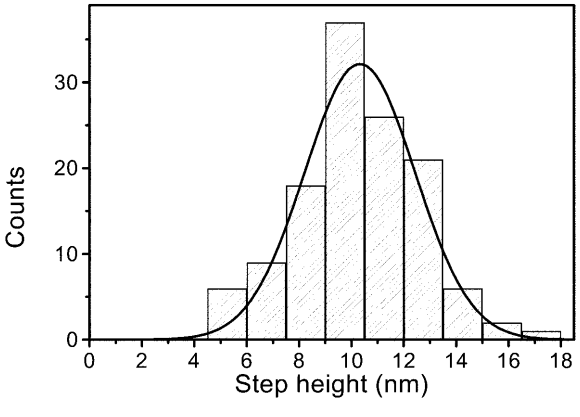


**Fig. 7** Histogram of the step height measured on different sections of raw height images. The total number of observations is 127. Sections were processed as described in Materials and methods in order to correct for the tilt of the crystal face. *Solid line*: Gaussian fit of the histogram, providing a step height of $10.5 \pm 0.6$ nm

A higher resolution image (area 450×400 nm$^2$) revealed fine details of the terraces, allowing us to observe the surface structure at the molecular level (Fig. 8). As expected for the (111) face of a fcc crystal, the surface molecular packing appears hexagonal. The lattice symmetry and spacing were measured by performing a two-dimensional Fourier transform analysis of image portions corresponding to single terraces. The lattice spacing turns out to be $13.1 \pm 0.3$ nm, corresponding to an area per oligomer of $149 \pm 3$ nm$^2$. The surface lattice spacing determined by Fourier analysis of the images is in good agreement with the surface lattice spacing of 13.0 nm calculated from the bulk lattice spacing measured by X-ray diffraction.

The study of step edge morphology allows us to obtain an order of magnitude estimate for the surface free energy, assuming that growth occurs by two-dimensional nucleation. The free energy change for nucleation may be given by (Sangwal 1994):

$$\Delta G = -V\Delta G_v + A\gamma \tag{1}$$

where $\gamma$ is the surface free energy, $V$ is the volume and $A$ the area of the nucleus. For a circular disc-shaped nucleus of height $h$ and radius $r$, Eq. (1) may be written as:

$$\Delta G = -\pi r^2 h\Delta G_v + 2\pi rh\gamma \tag{2}$$

Differentiating with respect to $r$ and equating to zero, a relation between $\gamma$ and the critical size of the nucleus is obtained:

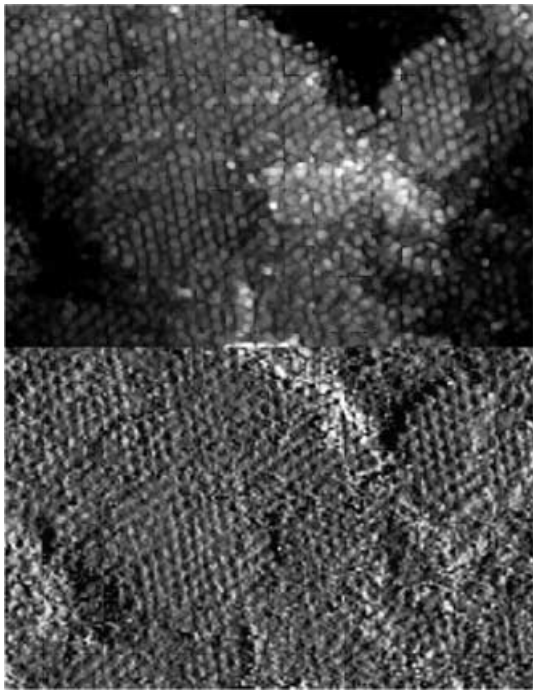

**Fig. 8** Tapping mode AFM image of a ferritin crystal (111) face at molecular resolution. Several monomolecular islands are visible. *Top*: height data, $z$ range 100 nm; *bottom*: amplitude data, $z$ range 2.1 nm. Image area 450×400 nm$^2$

$$\gamma = r_c\Delta G_v \tag{3}$$

Equation (3) holds in the case of isotropic growth and therefore it will be used in this work to evaluate $\gamma$ for ferritin crystals. On the other hand, for lysozyme, growth turned to be anisotropic. In this case, an elliptical nucleus rather than a circular one must be considered in Eq. (1):

$$\Delta G = -\pi xyh\Delta G_v + 4h\gamma x\int_0^{\pi/2}\sqrt{1 - e^2\sin^2\phi}\,\mathrm{d}\phi \tag{4}$$

where $x$ and $y$ are the major and minor semi-axes of the elliptical nucleus, respectively, and $e = \sqrt{1 - y^2/x^2}$ is the eccentricity. The AFM images show the occurrence of small elliptical nuclei whose size yields eccentricity values in the range between 0.8 and 0.9. The integral in Eq. (4) is reported in mathematical tables as a function of $\sin^{-1}e$. Since in the region of interest it shows a linear behavior, we replaced it with a linear function:

$$\Delta G = -\pi xyh\Delta G_v + 4\gamma hx\left(a - b\sin^{-1}\left(\sqrt{1 - y^2/x^2}\right)\right) \tag{5}$$

where the parameters $a$ and $b$ were obtained by a linear fit of the integral values reported in the tables. Differentiating with respect to $x$ and $y$ and equating to zero, two equations relating $\gamma$ to the critical size of the nucleus are obtained:

$$\gamma = \frac{\pi x_c\Delta G_v}{8b} \tag{6}$$

$$\gamma = \frac{\pi y_c\Delta G_v}{4\left(a - 2by_c/x_c - b\sin^{-1}\left(\sqrt{1 - y_c^2/x_c^2}\right)\right)} \tag{7}$$

These equations will be used to evaluate $\gamma$ from the measured size of the growth nuclei in lysozyme crystal faces.

$\Delta G_v$ depends on supersaturation according to the expression $\Delta G_v = kT\sigma/\Omega$, where $k$ is Boltzmann's constant, $T$ is the absolute temperature, $\sigma$ is the relative supersaturation and $\Omega$ is the molecular volume. The relative supersaturation is defined by $\sigma = ln(c/c_e)$, where $c$ is the actual protein concentration and $c_e$ is the equilibrium protein concentration. For lysozyme, the latter turns out to be 18 mg mL$^{-1}$ from data in the literature (Ries-Kautt and Ducruix 1992), while for ferritin it was determined to be 2.5 mg mL$^{-1}$ by absorption spectroscopy. An upper limit for $c$ is twice the initial protein concentration in the drop, which is 40 mg mL$^{-1}$ for lysozyme and 25 mg mL$^{-1}$ for ferritin. Therefore, $\sigma$ turns out to be 0.8 and 2.3, respectively. The molecular volume $\Omega$, calculated from the unit cell dimensions, is equal to $2.37\times10^2$ nm$^3$ in the case of lysozyme and $1.56\times10^3$ nm$^3$ for ferritin. For ferritin, an estimate for $r_c$ was obtained by measuring the radius of curvature at multiple points along the step edges, yielding $r_c = 32 \pm 8$ nm; therefore, we find from Eq. (3) that $\gamma = 0.19$ mJ m$^{-2}$.

For lysozyme, the size of the elliptical nuclei turned out to be $2x = 44 \pm 5$ nm and $2y = 24 \pm 5$ nm. Equations (6) and (7) yielded compatible values (within experimental errors) of $\gamma = 0.22$ mJ m$^{-2}$ and $\gamma = 0.20$ mJ m$^{-2}$, respectively. These values are comparable with those determined by AFM measurements on other macromolecular crystals (Land et al. 1995; Malkin et al. 1995), but turn out to be three orders of magnitude smaller than in a metal (Chernov 1984). This can be due to the high solvent content of protein crystals, which is 39.5% for lysozyme and 61.5% for ferritin, equivalent to protein concentrations of 0.056 M and 0.025 M, respectively. Therefore, since the crystal and the solution can be considered as nearly equivalent environments, the energy required to form surface states is relatively small compared to other solid state systems.

## Conclusions

We have used tapping mode atomic force microscopy to compare the surface structures of hen egg-white lysozyme and horse spleen ferritin crystals. The (101) face of lysozyme crystals and the (111) face of ferritin crystals were investigated. We found that these faces are characterized, respectively, by anisotropic and isotropic growth. The steps observed corresponded, for lysozyme, to monomolecular and bimolecular layers, whose thickness was $3.1 \pm 0.1$ nm and $6.7 \pm 0.2$ nm, respectively. For ferritin, monomolecular growth steps $10.5 \pm 0.6$ nm thick were present; the molecular packing of the terraces was hexagonal, as expected for the (111) face of a fcc crystal, with surface lattice spacing of $13.1 \pm 0.3$ nm. The surface free energy was determined by assuming that growth proceeds by nucleation, taking into account anisotropy in the case of lysozyme. The resulting values are in agreement with similar estimates obtained on other macromolecular crystals.

**Acknowledgements** The authors wish to express their thanks to Prof. Keshra Sangwal for helpful discussion. This work was supported by ASI contract I/R/28/00, CNR contract CT/02 PE/015186 "Sistemi per lo studio di proprietà fisiche di biomolecole" and MURST.

## References

Allen S, Chen X, Davies J, Davies MC, Dawkes AC, Edwards JC, Roberts CJ, Sefton J, Tendler SJB, Williams PM (1997) Detection of antigen-antibody binding events with the atomic force microscope. Biochemistry 36:7457–7463

Allen S, Chen X, Davies J, Davies MC, Dawkes AC, Edwards JC, Roberts CJ, Tendler SJB, Williams PM (1998) The application of force microscopy to immunodiagnostic systems imaging and biomolecular adhesion measurements. Appl Phys A 66:S255–S261

Barabási AL, Stanley HE (1995) Fractal concepts in surface growth. Cambridge University Press, Cambridge

Basu JK, Hazra S, Sanyal MK (1999) Growth mechanisms of Langmuir-Blodgett films. Phys Rev Lett 82:4675–4678

Chernov A (1984) Modern crystallography III. Springer, Berlin Heidelberg New York

Durbin SD, Carlson WE (1992) Lysozyme crystal growth studied by atomic force microscopy. J Cryst Growth 122:71–79

Durbin SD, Feher G (1990) Studies of crystal growth mechanisms of proteins by electron microscopy. J Mol Biol 212:763–774

Durbin SD, Carlson WE, Saros MT (1993) In situ studies of protein crystal growth by atomic force microscopy. J Phys D 26:B128–B132

Forsythe E, Ewing F, Pusey M (1994) Studies on tetragonal lysozyme crystal growth rates. Acta Crystallogr Sect D 50:614–619

Forsythe EL, Nadarajah A, Pusey ML (1999) Growth of (101) faces of tetragonal lysozyme crystals: measured growth-rate trends. Acta Crystallogr Sect D 55:1005–1011

Furuno T, Sasabe H, Ikegami A (1998) Imaging two-dimensional arrays of soluble proteins by atomic force microscopy in contact mode using a sharp supertip. Ultramicroscopy 70:125–131

Konnert JH, D'Antonio P, Ward KB (1994) Observation of growth steps, spiral dislocations and molecular packing on the surface of lysozyme crystals with the atomic force microscope. Acta Crystallogr Sect D 50:603–613

Land TA, Malkin AJ, Kuznetsov YuG, McPherson A, De Yoreo JJ (1995) Mechanisms of protein crystal growth: an atomic force microscopy study of canavalin crystallization. Phys Rev Lett 75:2774–2777

Land TA, De Yoreo JJ, Lee JD (1997) An in-situ AFM investigation of canavalin crystallization kinetics. Surf Sci 384: 136–155

Li H, Nadarajah A, Pusey ML (1999) Determining the molecular growth mechanisms of protein crystal faces by atomic force microscopy. Acta Crystallogr Sect D 55:1036–1045

Malkin AJ, Land TA, Kuznetsov YuG, McPherson A, De Yoreo JJ (1995) Investigation of virus crystal growth mechanisms by in situ atomic force microscopy. Phys Rev Lett 75:2778–2781

Malkin AJ, Kuznetsov YuG, McPherson A (1997). An in situ AFM investigation of catalase crystallization. Surf Sci 393: 95–107

Malkin AJ, Kuznetsov YuG, McPherson A (1999) In situ atomic force microscopy studies of surface morphology, growth kinetics, defect structure and dissolution in macromolecular crystallization. J Cryst Growth 196:471–488

Nadarajah A, Pusey ML (1996) Growth mechanism and morphology of tetragonal lysozyme crystals. Acta Crystallogr Sect D 52:983–996

Ohnishi S, Hara M, Furuno T, Sasabe H (1992) Imaging the ordered arrays of water-soluble protein ferritin with the atomic force microscopy. Biophys J 63:1425–1431

Ohnishi S, Hara M, Furuno T, Okada T, Sasabe H (1993) Direct visualization of polypeptide shell of ferritin molecule by atomic force microscopy. Biophys J 65:573–577

Perrin A, Lanet V, Theretz A (1997) Quantification of specific immunological reactions by atomic force microscopy. Langmuir 13:2557–2563

Ries-Kautt M, Ducruix A (1992) Phase diagrams. In: Ducruix A, Giegé R (eds) Crystallization of nucleic acids and proteins: a practical approach. Oxford University Press, Oxford, pp 195–218

Sangwal K (1994) Kinetics and mechanisms of crystal growth. In: Sangwal K (ed) Elementary crystal growth. Saan Publishers, Lublin, Poland, pp 83–176

Yip CM, Ward MD (1996). Atomic force microscopy of insulin single crystals: direct visualization of molecules and crystal growth. Biophys J 71:1071–1078

Yip CM, Brader ML, Ward MD, DeFelippis MR (1998a) Atomic force microscopy of crystalline insulin: the influence of sequence variation on crystallization and interfacial structure. Biophys J 74:2199–2209

Yip CM, DeFelippis MR, Frank BH, Brader ML, Ward MD (1998b) Structural and morphological characterization of ultralente insulin crystals by atomic force microscopy: evidence of hydrophobically driven assembly. Biophys J 75:1172–1179